INSTITUTE OF PHYSICS PUBLISHING SEMICONDUCTOR SCIENCE AND TECHNOLOGY

Semicond. Sci. Technol. **20** (2005) 250–255 doi:10.1088/0268-1242/20/2/026

Deep level transient spectroscopy studies on $BaTiO_3$ and $Ba_{1-x}Ca_xTiO_3$ thin films deposited on Si substrates

P Victor and S B Krupanidhi

Materials Research Center, Indian Institute of Science, Bangalore 560 012, India

E-mail: victor@mrc.iisc.ernet.in

Received 29 November 2004, in final form 1 December 2004
Published 20 January 2005
Online at stacks.iop.org/SST/20/250

Abstract

Laser ablation grown $BaTiO_3$ and $Ba_{1-x}Ca_xTiO_3$ thin films were studied in the metal–ferroelectric–semiconductor configuration by the deep level transient spectroscopy (DLTS) technique. The capture cross section, bulk and interface traps were determined from the DLTS technique. The distributions of calculated interface states were mapped with the silicon energy band gap for both the thin films. The interface states of the $Ba_{1-x}Ca_xTiO_3$ thin films were found to be higher than the $BaTiO_3$ thin films. The substitution of Ca^{2+} into the Ba^{2+} sites of $BaTiO_3$ results in a decreased lattice constant, thereby leading to shrinkage in the unit cell. This might be one of the reasons for the higher density of interface states present in $Ba_{1-x}Ca_xTiO_3$, as it leads to a large number of unsaturated bonds at the interface of Si substrate–thin films. The calculated capture cross section of the interface traps in both the $BaTiO_3$ and $Ba_{1-x}Ca_xTiO_3$ thin films was very low in the range of 10^{-21} cm^2.

1. Introduction

In recent years, the popularity of ferroelectric random access memories had led to extensive research on metal–ferroelectric–insulator–semiconductor (MFIS), MFS or MFS field effect transistor (MFSFET) structures [1, 2]. The MFSFET structure has the unique capability of shrinking memory cell dimensions. The advantage of using ferroelectric thin films over linear dielectrics is that the charge is induced by remanent polarization in ferroelectric materials, which controls the surface conductivity of the Si substrates. Pb(Zr, Ti)O_3, $PbTiO_3$ and $SrBi_2Ta_2O_9$ are the popular ferroelectric thin films deposited on Si substrate in recent years [3, 4]; however, the quest for other non-Pb-based compounds is in progress [5]. Specifically, barium titanate and isovalent substituted $BaTiO_3$ are the promising candidates for potential use in applications to ferroelectric memories, microwave communications and optoelectronic devices. Barium calcium titanate (BCT) crystals show potential for applications in advanced laser systems, optical interconnects and optical storage devices [6]. Calcium acts as a reduction inhibitor in $BaTiO_3$ and reduces the possibility of formation of unwanted hexagonal phase and the BCT properties are strongly dependent on processing parameters [7]. MFIS or MFS structures will exhibit good memory characteristics based on numerous factors, the most important being to exhibit good interface properties. Hence, it is essential to carry out an extensive investigation at the thin film–Si substrate interface. The deep level transient spectroscopy (DLTS) technique [8] was initially used to probe into bulk traps in p–n junctions or Schottky barriers [9, 10] and MOS structures [11, 12], and was recently used in MFS capacitors [13]. There are very few reports on the DLTS technique based on ferroelectric thin films [13, 14]. This technique is essential as it provides reliable information on the interface states, especially in the vicinity of the band edges, because the transient capacitance measured from DLTS is independent of surface potential fluctuation in MOS structures. In this paper, we report on the investigation of interface and bulk states, and on the capture cross section in $BaTiO_3$ and $Ba_{1-x}Ca_xTiO_3$ ($x = 0.05$, 0.08 and 0.1) thin films on p-type Si substrate using the DLTS technique.

2. Experiment

$BaTiO_3$ (denoted as BT) and $Ba_{1-x}Ca_xTiO_3$ targets ($x = 0.05$, denoted as BCT5; 0.08 and 0.10 (BCT10)) were prepared via the conventional solid state reaction method. High-purity starting powders of $BaCO_3$, TiO_2 and $CaCO_3$ were weighed in stoichiometric proportion, ball milled for 20 h, dried and calcined at 1100 °C for 3 h. The calcined powders were pressed at 100 kN cm^{-2} into a 15 mm diameter disc shaped pellet and the pellets were sintered at 1400 °C for 4 h. The density of targets was 96% and these $Ba_{1-x}Ca_xTiO_3$ and $BaTiO_3$ targets were used for the laser ablation. The BCT thin films were deposited on the p-type Si substrate ($\rho \sim 7$–15 Ω^{-1} cm^{-1}) using the KrF excimer laser ablation technique (Lambda Physik 248 nm). The substrate temperature during the deposition was maintained at 700 °C, with laser fluence maintained at 3 J cm^{-2} and the substrate–target distance at 3.5 cm. The base pressure was initially brought down to 1×10^{-6} Torr and prior to the deposition, high purity oxygen gas was introduced into the chamber and the BT and BCT thin films deposition was carried out at 100 mTorr. The *in situ* grown thin films and targets were structurally characterized by x-ray diffraction (XRD). The composition and distribution of the elements in thin films across the thickness were identified using energy dispersive analysis (EDAX) and secondary ion mass spectroscopy (SIMS), respectively. The surface morphology of all thin films was done using a scanning electron microscope (SEM). Different sized top electrodes of Au circular dots of area 2×10^{-2} cm^2 and 1.96×10^{-3} cm^2 were sputtered for the fabrication of the MFS capacitor. The electrode annealing was carried out at 325 °C for 15 min and the MFS capacitor was used for the DLTS characterization. Dielectric and capacitance–voltage (C–V) measurements were measured using an impedance analyser HP 4284 A at frequencies ranging from 40 Hz to 1 MHz at room temperature. DLTS measurements were performed on MFS capacitors with a double boxcar averager system operating at 1 MHz and the DLTS spectrum was recorded between 80 and 300 K for different time constants ranging from 1 to 800 ms^{-1}.

3. Results and discussion

3.1. Phase and stoichiometric determination

Figure 1 shows the x-ray diffraction pattern of BT and BCT10 thin films. The BCT10 thin films exhibit a distinct tetragonal splitting at (200/002) showing the pure perovskite phase formation. The BT thin films also exhibit an excellent polycrystalline nature with sharper and more intense peaks. There was no secondary phase formation observed in these thin films. The thickness of thin films varied from 200 to 300 nm as measured by the Stylus method (Dektek). Figure 2 shows the SIMS analysis of BCT5 thin films deposited on Si substrate and shows that there exists a sharp film–substrate interface and a uniform distribution of elements throughout the films. The EDAX showed excellent stoichiometry maintained in $BaTiO_3$ and $Ba_{1-x}Ca_xTiO_3$ ($x = 0.05$, 0.08 and 0.1) thin films. The surface morphology obtained from the SEM was found to be a smooth surface and the grains were dense with minimal pores, showing that the thin films grown by pulsed excimer laser ablation were very good.

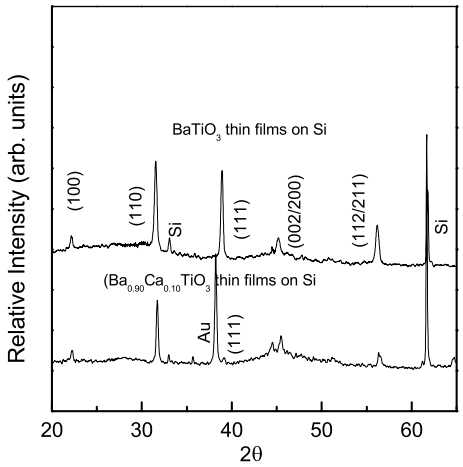

Figure 1. X-ray diffraction pattern of polycrystalline $BaTiO_3$ and $(Ba_{0.9}Ca_{0.1})TiO_3$ thin films.

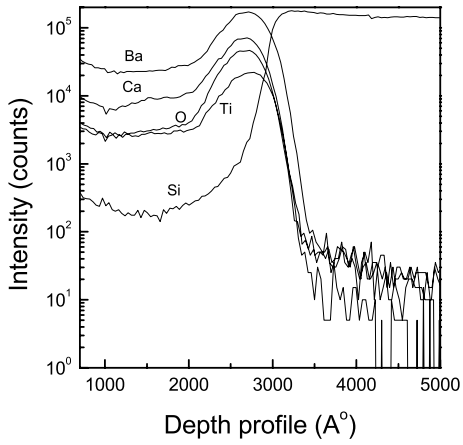

Figure 2. SIMS analysis of the BCT5 thin films deposited on the Si substrate.

3.2. Capacitance–voltage measurements

The C–V measurements were carried out on the MFS capacitors at room temperature, with a superimposed sinusoidal amplitude voltage of 500 mV at 1 MHz. Figure 3 shows the dielectric constant versus gate voltage of the BT and BCT10 thin films. The dielectric constant is deduced from the capacitance of the C–V curve and sweeping the bias gate voltage from negative to positive and back, resulting in a C–V clockwise hysteresis loop. This hysteresis effect shows the signature of the presence of ferroelectric material playing its role [15]. The hysteresis displays an excellent memory window in both the BT and BCT thin films of 2 and 1 V loop widths, respectively. The C–V measurement was repeated for various ramp rates ranging from 0.05 V s^{-1} to 1.1 V s^{-1} at room temperature at 1 MHz, and the resulting hysteresis curve remained unchanged, confirming that the mobile ions did not participate and it is the ferroelectricity of the BT or BCT10 thin films playing the dominant role [16]. The interface states calculated from C–V measurements for the BT and BCT10 thin films were 4.75×10^{10} and 2.62×10^{11} eV^{-1} cm^{-2}, respectively [17]. The dielectric constant ($\varepsilon^{|}$) was calculated in the accumulation region and with the increase in the Ca

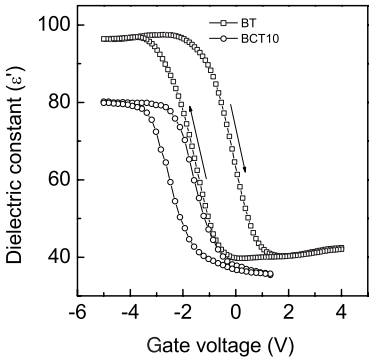

Figure 3. Hysteretic behaviour measured by the *C–V* technique of the ferroelectric BT and BCT10 thin films on p-type Si substrate.

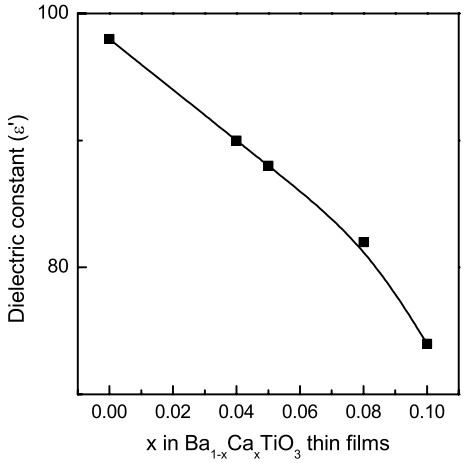

Figure 4. Decrease of dielectric constant ($\varepsilon^{|}$) as a function of Ca substitution in the $BaTiO_3$ thin films.

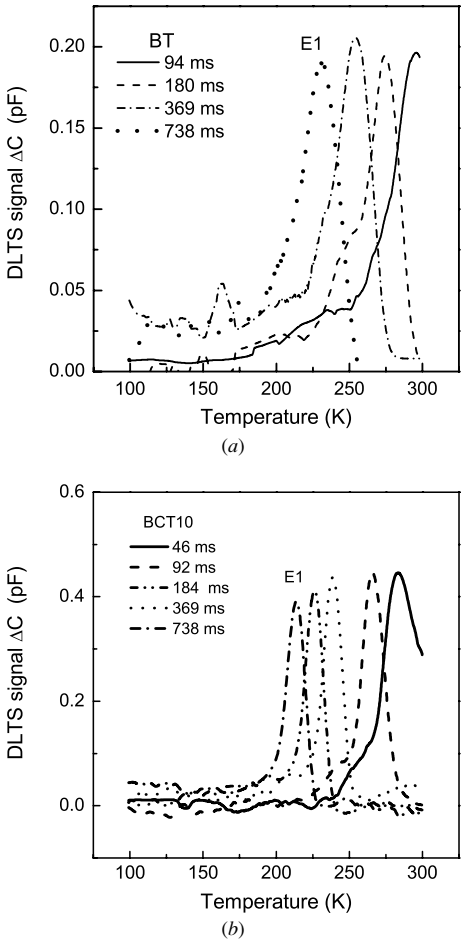

Figure 5. DLTS spectrum of (*a*) BT and (*b*) BCT10 thin films in the MFS capacitor configuration.

content, the dielectric constant ($\varepsilon^{|}$) was observed to decrease and is shown in figure 4. This is attributed to the shrinkage of the lattice constant in the unit cell on substitution of Ba^{2+} by smaller ionic radii Ca^{2+}. Such shrinkage results in the decrease in motion of Ti^{4+} ions in the octahedral cage, thereby resulting in the decrease of dielectric constant ($\varepsilon^{|}$). This replacement of Ba^{2+} with smaller Ca^{2+} 'tightens' the structure making it difficult to remove the oxygen from the lattice and making it more favourable to fill the extrinsic oxygen vacancies.

3.3. DLTS studies

A quiescent voltage (V_d) with a filling metal semiconductor bias (V_f) of large duration (t_p) is applied to a MFS capacitor [12, 15]. A detailed description on the principle of DLTS and its operation on MOS capacitors is given elsewhere [18, 19]. Figures 5(*a*) and (*b*) show the DLTS spectra of the BT and BCT10 thin films in the MFS capacitor configuration, recorded at various temperatures ranging from 80 K to 300 K. The emission rate window peaks are sharper indicating the existence of discrete interface trap levels in all the analysed MFS capacitors. The correlation signal of the peak E1 (labelled in figures 5(*a*) and (*b*)) in both the BT and BCT10 thin films increased with an increase in the quiescent bias voltage (V_d) in the positive direction and is due to the minority carrier trapping effects (electron traps). Figures 6(*a*) and (*b*) show the DLTS spectra of BT and BCT10 thin films measured at a fixed quiescent bias voltage (V_d) for different filling biases (V_f). The DLTS signal peak was observed to be discrete, sharp and found to shift with the temperature, showing the presence of more traps contributing to the DLTS signal as pulse height increases. The spatial localization at the interface confirms that the traps are due to the interface states. When the minority carriers capture dominates, at higher temperatures, the correlation signal is given by [20]

$$C_s(t_1, T) = A\exp(-c_n t_1)[1 - \exp(-c_n t_1)]\int_{E_V}^{E_F} N_{ss}\,dE \quad (1)$$

where N_{ss} is the density of interface states, $n_s c_n$ is the electron capture and t_1 is the time of transient capacitance value. The onset of minority carrier trapping at higher temperatures has been observed from the slower set of gate delay times. At higher temperatures and with slower gate delay times, a large peak was observed, which is expected for the minority carrier trapping. A strong bias dependence is observed for the position and shape of this peak, which supports the minority carrier trapping effects. The sharp intense peak denoting minority carrier capture is observed and is typically observed only in the p-type materials [21]. The presence of a minority carrier trap may be due to a surface inversion layer created in p-type Si while applying the reverse bias during the measurements

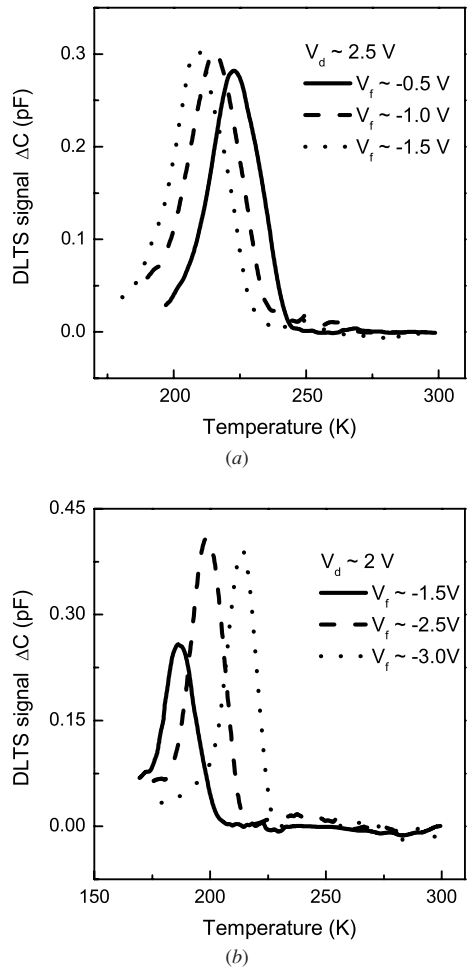

Figure 6. DLTS spectra of (*a*) BT and (*b*) BCT10 thin films measured at a fixed quiescent bias voltage V_d for different filling biases V_f.

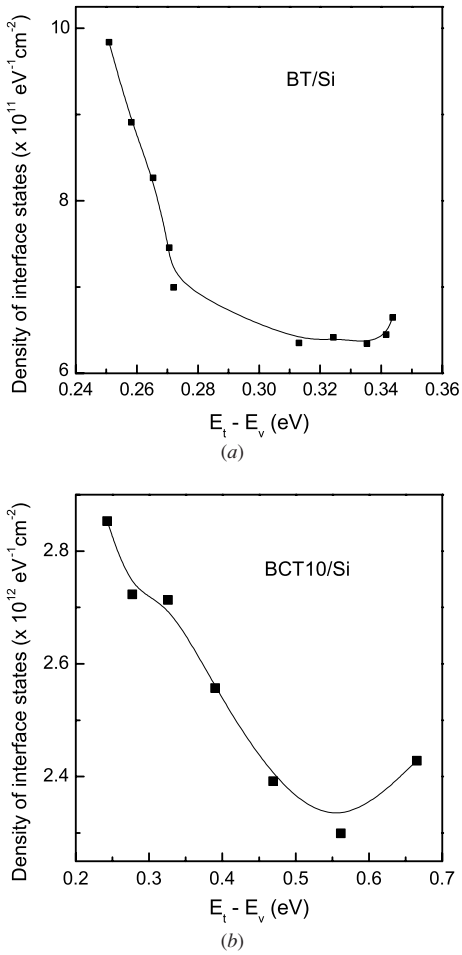

Figure 7. The distribution of interface traps for (*a*) BT and (*b*) BCT10 thin films.

and/or due to the domination of minority carrier capture at higher temperatures. At this inversion condition, the minority carriers will be injected into the space charge region and will fill the states in the band gap of the semiconductor. There are reports in the literature that the minority carrier capture may replace the expected majority carrier emission process if temperature and other factors are favourable [20, 21]. It also implies that sufficient electrons become available for capture by the electron traps for electron emission. This explicitly shows that all the measured MFS capacitors in our case display the minority capture effect.

The interface trap density (N_{ss}) as a function of energy trap levels (E_t) in the band gap of Si can be deduced from the DLTS spectrum using relations (2) and (3)

$$N_{ss}(E_t) = \Delta C \frac{C_{ox}}{C_q^3} \frac{\varepsilon_s}{kT \ln(t_2/t_1)} N_A \tag{2}$$

$$E_t = E_v + \frac{kT}{q} \ln\left(\sigma_p v_{th} N_v \frac{t_2 - t_1}{\ln(t_2/t_1)}\right) \tag{3}$$

where ΔC is the DLTS signal i.e. the difference in the transient capacitance values at times t_1 and t_2, T is the temperature and C_q is the capacitance of MFS measured at V_d. The density of interface states and the distribution of interface states in the silicon energy band gap were calculated for the BT and BCT10 thin films using equations (2) and (3), respectively. The distribution was determined from the ΔC versus T plot, on assuming an energy independent capture cross section. The interface trap distribution within the lower half of the band gap for the BT and BCT10 thin films is shown in figures 7(*a*) and (*b*), respectively. The shape of N_{ss} calculated from DLTS is observed to decrease towards the mid-band gap in both the cases of BT and BCT10 thin films and then slightly increase at the edges, exhibiting the typical 'U' shape in the N_{ss} distribution [22]. It has been observed that the N_{ss} values calculated from the DLTS were observed to be higher than the C–V measured N_{ss} values, as the DLTS takes into account the complete filling of the traps and also efficiently takes the slightest variation of surface potential fluctuations into account.

The BCT10 thin films were found to exhibit higher interface states than BT thin films. The density of interface states (D_{it}) was observed to increase with an increase in Ca^{2+} substitution in Ba^{2+} sites of $BaTiO_3$ thin films. The substitution of smaller ionic radii Ca^{2+} in Ba^{2+} sites of $BaTiO_3$ results in a decrease of the lattice constant leading to the shrinkage of the unit cell in $Ba_{1-x}Ca_xTiO_3$. Such shrinkage of the lattice constant results in a large number of unsaturated bonds leading

Table 1. The various trap parameters obtained from the DLTS spectra for both BCT and BT thin films.

$Au/BaTiO_3$/p-type Si			$Au/Ba_{0.9}Ca_{0.1}TiO_3$/p-type Si		
Gate voltage (V)	Capture cross section (σ_p) × 10^{-21} cm^2	ΔE_σ (eV)	Gate voltage (V)	Capture cross section (σ_p) × 10^{-21} cm^2	ΔE_σ (eV)
−0.5	5.92	0.101	−1.7	4.145	0.135
−1.0	1.43	0.085	−2.5	6.796	0.1
−1.7	0.178	0.31	−3.0	3.789	0.13

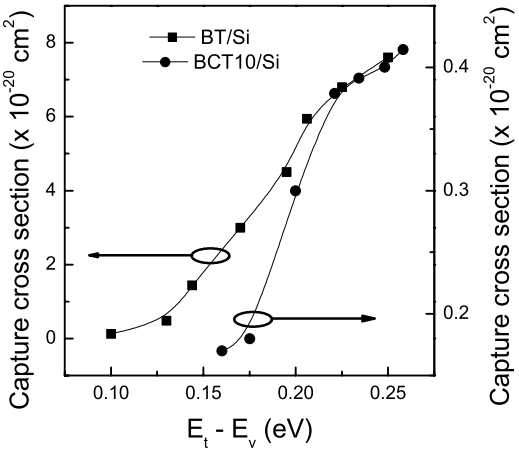

Figure 8. Capture cross section of the interface states in BT and BCT10 thin films.

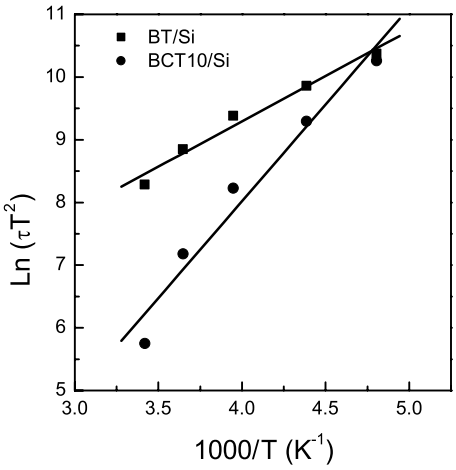

Figure 9. Arrhenius plot of $\ln(\tau T^2)$ versus $1000/T$ for the bulk traps in BT and BCT10 thin films.

to a significant number of interface states at the interface of BCT10/Si compared to BT/Si capacitors.

The capture cross section can be determined from the Arrhenius plots of thermal emission rate for the individual peak of the BT and BCT10 thin films with temperature. The energy level and capture cross section were calculated by the least-squares method taking into account the T^2 dependence of $v_n N_c$. The distribution of capture cross section σ_p [23] is obtained from the temperature scan DLTS technique and the temperature dependence of capture cross section exhibits an exponential nature as follows:

$$\sigma_p(E, T) = \sigma_o(E) \exp\left(-\frac{\Delta E_\sigma(E)}{kT}\right) \tag{4}$$

where σ_o and ΔE_σ are constants inherent to the trap. On further simplifying equation (4), the following expression is obtained

$$e_p = \sigma_o v_{th} N_a \left(\frac{T}{300}\right)^{1/2} \exp\left(-\frac{(q\psi_s + \Delta E_\sigma)}{kT}\right) \tag{5}$$

with N_a and ψ_s denoting bulk doping density of Si and surface band bending, respectively. A temperature scan of the correlation signal displays a large narrow peak, while an energy-dependent capture cross section will broaden the peak. The calculated capture cross section for the BT thin films as shown in figure 8 was of the order of 10^{-20}–10^{-21} cm^2 in the energy range from $E_v + 0.05$ V to $E_v + 0.12$ eV, by changing the filling bias voltage from −1.0 V to 1.5 V at the fixed voltage in the capture process of $V_d = 2$ V. Similarly for the BCT10 thin films, the capture cross section is shown as a function of $E_t - E_v$ in figure 8. The obtained capture cross section values are found to be very small and these low capture cross section values together with the increase of σ_p with the energy levels ($E_t - E_v$) further confirm that the minority carrier capture is the most dominant process near the midgap. The calculated ΔE_σ is quite reasonable with the earlier reported values [24, 25] and is shown in table 1.

The capture cross section for electron emission and capture is strongly dependent on temperature at the interface and can be explained by the lattice-relaxation multiphonon emission model [23]. This model was proposed based on the temperature variation of the capture cross section of bulk levels in polar semiconductors such as GaAs and GaP. This model assumes a neutral centre (acceptor near conduction band, donor near valence band) in which the vibrations of a single lattice coordinate linearly modulate along the depth of the potential well binding the carrier. Here the capture results from the lattice vibrations causing the crossing of free and bound carrier levels. Immediately after capture, the vibrations about the new equilibrium position will be rapidly damped (i.e., the lattice equilibrium position changes) leaving the captured carrier in a highly excited vibrational state which rapidly decays into the equilibrium state by multiphonon emission. Multiphonon emission has its largest temperature dependence above the room temperature where the cross section can often be expressed in the form given by equation (5), thereby a implying that ΔE_σ is positive. The general behaviour of the valence band interface states is consistent with the freeze-out of the capture cross section in the lattice relaxation model for multiphonon emission. This type of behaviour was first observed by Schulz and Johnson in metal-SiO_2-n-type Si capacitors [20].

The corresponding DLTS signal from the interface traps can be suppressed by always maintaining the surface in depletion so that the interface traps are never filled and

increasing the reverse bias, thereby a larger depletion depth can be explored and the volume traps or bulk traps can be detected. It is interesting to observe that in the case of the bulk traps, the peak temperature of the DLTS signal does not change with pulse height, since the emission rate at a particular temperature is constant regardless of the pulse height. The volume trap located at $E_t \sim 0.14$ eV and 0.24 eV for the BT and BCT10 thin films from the valence band, respectively, was calculated from the Arrhenius plot shown in figure 9. The BT and BCT crystals can have several kinds of defects such as Schottky defects, Frenkel defects and nonstoichiometry. Baetzold [25] suggested that vacancies at the Ba and Sr sites are the most prevalent trap sources in the SBN single crystal because the vacancies have a relatively small defect energy of 0.3 eV per defect. Hence, our bulk trap activation energies suggest the possibility of the cation vacancies playing their part at their respective sites.

4. Conclusion

The interface states and capture cross section were measured by the DLTS technique and the density of interface states of the $BaTiO_3$–Si capacitors was lower than that of the $Ba_{0.9}Ca_{0.1}TiO_3$–Si capacitors. This was attributed to the shrinkage of the lattice constant due to the substitution of Ca^{2+} in Ba^{2+} sites. The peaks observed in both cases of BT and BCT10 thin films were due to the minority carrier traps. The calculated capture cross sections of the minority carrier trap values were low for both the BT and BCT10 thin films.

Acknowledgment

One of the authors (P Victor) wishes to acknowledge the Council for Scientific Industrial Research (CSIR-SRF) for the graduate fellowship.

References

[1] Park B H *et al* 1999 *Nature* **401** 682
Ishiwara H 2000 *FED J.* **11** 27
[2] Scott J F 2000 *Ferroelectric Memories* (Berlin: Springer)
Paz de Araujo C A, Cuchiaro J D, McMillan L D, Scott M C and Scott J F 1995 *Nature* **374** 627
[3] Shichi Y, Tanimoto S, Goto T, Kuroiwa K and Tarui Y 1994 *Japan. J. Appl. Phys.* **33** 5172
[4] Prins M W J, Zinnermers S E, Cillessen J F M and Giesbers J B 1997 *Appl. Phys. Lett.* **70** 458
[5] Yoshimura T, Fujimura N and Ito T 1995 *Appl. Phys. Lett.* **66** 221
[6] Veenhuius H *et al* 2000 *Appl. Phys.* B **70** 797
[7] Tiwari V S, Phandey D, Krishna P S R, Chakravarthy R and Dasanacharya B A 1991 *Physica* B **172** 112
[8] Lang D V 1974 *J. Appl. Phys.* **45** 3023
[9] Evwraye A O and Sum E 1976 *J. Appl. Phys.* **47** 3172
[10] Nagasawa K and Schulz M 1975 *Appl. Phys.* **8** 35
[11] Murray F, Carin R and Bogdanski P 1986 *J. Appl. Phys.* **60** 3592
[12] Yamasaki K, Yoshida M and Sugano T 1979 *Japan. J. Appl. Phys.* **18** 113
[13] Yang Y S *et al* 2000 *Appl. Phys. Lett.* **76** 3472
[14] Wang Y P and Tseng T Y 1997 *J. Appl. Phys.* **81** 6762
[15] Ito K and Tsuchiya H 1977 *Solid State Electron.* **20** 529
[16] Han J P and Ma T P 1998 *Appl. Phys. Lett.* **72** 1185
[17] Victor Louis Arockiaraj P 2004 *PhD Thesis* Indian Institute of Science, Bangalore, India
[18] Ozder S, Atilgan I and Katicioglu B 1996 *Solid State Electron.* **39** 243
[19] Tredwell T J and Viswanathan C R 1980 *Solid State Electron.* **23** 1171
[20] Schulz M and Johnson N M 1978 *Solid State Commun.* **25** 481
[21] Schulz M and Johnson N M 1977 *Appl. Phys.* **31** 622
[22] Nicollian E H and Brews J R 1982 *MOS (Metal-Oxide Semiconductor) Physics and Technology* (New York: Wiley)
[23] Katsube T, Kakimoto K and Ikoma T 1981 *J. Appl. Phys.* **52** 3504
[24] Ozder S, Atilgan I and Katicioglu B 1995 *Semicond. Sci. Technol.* **10** 1510
[25] Baetzold R C 1993 *Phys. Rev.* B **48** 5789